J. APPLIED FIRE SCIENCE, Vol. 9(4) 311-345, 1999-2000

THE DEVELOPMENT OF A CFD BASED SIMULATOR FOR WATER MIST FIRE SUPPRESSION SYSTEMS: THE DEVELOPMENT OF THE FIRE SUBMODEL

R. N. MAWHINNEY

A. J. GRANDISON

E. R. GALEA

M. K. PATEL

J. EWER

University of Greenwich, London

ABSTRACT

The FIRE Detection And Suppression Simulation (FIREDASS) project was concerned with the development of water misting systems as a possible replacement for halon based fire suppression systems currently used in aircraft cargo holds and ship engine rooms. As part of this program of work, a computational model was developed to assist engineers optimize the design of water mist suppression systems. The model is based on Computational Fluid Dynamics (CFD) and comprised of the following components: fire model; mist model; two-phase radiation model; suppression model; detector/ activation model. In this paper the FIREDASS software package is described and the theory behind the fire and radiation sub-models is detailed. The fire model uses prescribed release rates for heat and gaseous combustion products to represent the fire load. Typical release rates have been determined through experimentation. The radiation model is a six-flux model coupled to the gas (and mist) phase. As part of the FIREDASS project, a detailed series of fire experiments were conducted in order to validate the fire model. Model predictions are compared with data from these experiments and good agreement is found.

1 INTRODUCTION

The advent of the Montreal Protocols (1986) where a world-wide ban on the production and use of Chlorofluorocarbons (CFCs) [1] was agreed has generated an urgent requirement for alternative fire control and suppression systems. This requirement is particularly urgent for aircraft manufacturers and operators who use halon based suppression and extinguishment systems exclusively in aircraft cargo holds due to their light weight and proven effectiveness. The worlds aviation industry has therefore been investigating alternative suppression systems, including powders, other gases, and water mist.

An associated problem with aircraft fire safety concerns the fire detection systems installed in aircraft cargo holds. Currently approximately 95 percent of all reported smoke warnings are false alarms [2]. Thus, if a water mist system were selected as a replacement for halon, improved detection systems would be essential in order to improve reliability and reduce the likelihood of unnecessary activations. In addition, an improved detection system could be used by an intelligent activation system to target the delivered water to the appropriate location, thereby assisting in the optimization of the overall system.

The FIREDASS research project was a European Union funded BRITE/EuRam research project set up to address this requirement for alternative suppression and improved detection systems [3-18]. Its specific aim was to develop a combined system comprised of a fine water mist suppression system, an improved detection system, and an intelligent control system for aircraft cargo holds. However, the task of developing an optimized version of such a system would require extensive physical experimentation and hence significant costs. Thus, one of the objectives of the FIREDASS project was to develop sophisticated engineering computational modeling tools which could be used both in the project and later routinely by industry to optimize such combined systems. This would allow the necessary physical experimentation to be better targeted and thereby reduce development time and cost.

Such a computational model has been developed. It was tested and validated by comparing its predictions with the results of a series of fire tests performed as part of the project. These included full-scale tests in an A-340 cargo test cell. This paper is the first in a series that describes this computational model and the results obtained in its validation. In this paper we detail its components, the submodels (section 2) and present in detail the development and validation of the Computational Fluid Dynamics (CFD) [19] based fire submodel [20, 21] and radiation submodel [22-25] at its heart (section 3).

The FIREDASS research project was run by the FIREDASS consortium which was comprised of the following partners: GEC Marconi Avionics (GMAv, U.K.), now BAe Systems; Cerberus Guinard (CG, France), now Siemens Cerberus; SINTEF NBL (SINTEF, Norway); University of Greenwich (UoG, U.K.); National Technical University of Athens (NTUA, Greece); DLR (DLR,

Germany); and the U.K. Civil Aviation Authority (CAA, U.K.). The FIREDASS research project was sponsored by the European Commission under BRITE/ EuRam Framework IV (contract no. BRPR-CT95-0040) and ran from February 1996 to February 1999.

2 STRUCTURE OF THE FIREDASS COMPUTATIONAL MODEL

The primary aim of the computational model development component of the FIREDASS research project was to generate and validate a number of submodels which, when integrated with a CFD engine, would allow the simulation of the interaction of fire, thermal radiation, and water mist with the detection and activation systems and with each other. The complete, integrated model would be able to address a number of different compartment configurations, primarily representing aircraft cargo holds but with possible extensions to other configurations such as ship engine rooms. The fire types that the model needed to address were gas burner fires, pool fires, and fire loads generated by cardboard boxes stuffed with shredded paper.

The submodels developed during the project were developed as separate computational modules. They were: the fire module (developed by UoG); the two-phase thermal radiation module (developed by NTUA); the water-mist module (developed by UoG); the fire suppression module (developed by SINTEF and UoG); and the detector/activation module (developed by CG). The framework for the computational model and the integration of the additional modules with the CFD engine was the responsibility of UoG. The modules were integrated through the CFD environment provided by the commercial software CFX 4.1 [26]. The interactions between the submodels are shown in Figure 1 and the submodels were as follows.

The fire submodel simulates the fire [4]. It supplies heat, smoke, and gaseous combustion product (CO_2, CO, H_2O, and O_2) production-consumption rates to the CFD engine. These rates are not predicted by the fire submodel but are provided as inputs from rate tables held in external files. These files contain data generated from experimental test fires for various types of fuel under various test conditions [3]. The test fires were part of a test series undertaken by SINTEF as part of the project. It is necessary to prescribe experimental data as the present fire submodel does not perform combustion calculations. The inclusion of complex combustion models, while possible, was not considered viable for use in this engineering model. The fire submodel is described further in section 3.1.

The fire suppression submodel was developed by UoG using an empirical criterion derived by SINTEF [9, 27]. By considering the average temperature and oxygen concentration of the air entrained into the fire it determines the point at which the fire is extinguished. This information is passed to the fire submodel which subsequently reduces the heat release rates.

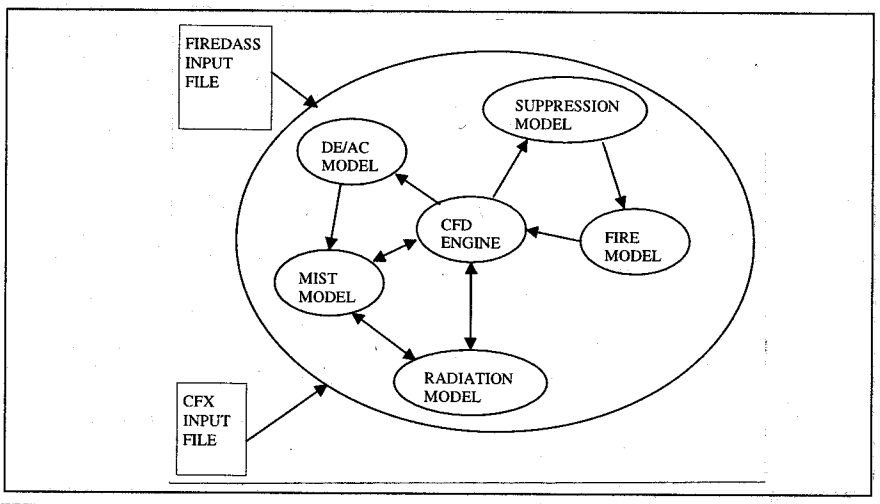

Figure 1. Interactions between FIREDASS submodels.

The detection/activation (DE/AC) submodel monitors the state of the environment (i.e., smoke concentrations and temperature) within the compartment and simulates the response of the sensors. With the predicted sensor responses, the activation routine determines which of the spray nozzles are to be activated and the nature of the pulsed activation sequence [10]. This information is passed to the mist submodel which generates the mist.

The mist submodel simulates the behavior of the water mist and its interaction with the fire atmosphere and the radiation field [5]. It determines the effect of the mist upon the temperature distribution within the compartment during the course of the fire. The mist submodel can support any number of nozzles that are activated by the DE/AC submodel though it does not predict the formation of the mist by the nozzle. The initial state of the mist was determined experimentally and is provided to the mist submodel as input parameters [28]. The mist submodel uses an Euler-Lagrange methodology, is transient and three-dimensional and fully two-way couples momentum, heat and mass using the PSI-Cell method [29]. Heat transfer includes exchange of heat with the radiation field. This is achieved by the mist submodel passing a summary of the mist to the radiation submodel which uses it to calculate how much heat the mist absorbs from the radiation field. These heat sources are then passed back to the mist submodel which applies them to the mist. Note that the mist also interacts with the fire through the suppression submodel, though only indirectly. The mist submodel will be the subject of a later publication [29] and is covered elsewhere [5, 9] so it will not be described in this paper.

The radiation submodel simulates the fire generated radiation field in the compartment and its interactions with the air, smoke, water mist, and compartment surfaces [8, 31]. It is a multiphase model based on the six-flux radiation model [22-25]. The heat sources representing the interaction of the radiation field with the air and smoke are passed directly to the CFD engine. The heat sources representing the interaction with the mist are passed to the mist submodel. The radiation submodel is described further in section 3.2 and in another publication [31].

The CFD engine used is CFX 4.1 [26]. This provides the computational models which convect and diffuse the fire products through the compartment, i.e., which calculate the fluid interactions. It also provides the framework for linking in the FIREDASS interface routines. These latter are routines which sit between the CFD engine and the FIREDASS modules and link them together. By accessing the CFX data structures and converting them to the data structures used in the FIREDASS modules and vice versa they also maintain the independence of the FIREDASS modules from the CFD engine and permit a highly modular structure to be adopted for the overall package. In principle, it should only be necessary to modify these interface routines to allow the FIREDASS modules to be ported to other CFD engines.

In the remaining sections of this paper, the fire and radiation submodels will be described in detail along with their testing and validation.

3 THE FIRE AND RADIATION SUBMODELS

Simulation of fire growth and spread within enclosures is a difficult task. The computer model must contend with the interaction between turbulence, gas-phase combustion, solid-phase combustion, and radiation. Over the past 15 years considerable effort has been expended in developing fire field models capable of predicting the development of hazardous conditions within fire enclosures [20, 21, 32-44]. At the heart of these fire field models are CFD codes and a large proportion of these models are based on commercial CFD software such as CFX 4.1 [26]. This code has been used in a number of fire modeling applications, for example, in the Kings Cross Underground fire [34] investigation, as well as aircraft and high rise building fire scenarios [35]. The majority of practical fire modeling applications have been concerned with the spread of heat and smoke in complex structures and so combustion has either been ignored or greatly simplified. In cases where combustion is ignored the fire is treated as a simple prescribed source of heat and smoke. While this approximation may appear crude it can produce good agreement with experimentally derived temperature measurements [36-38] for room fire scenarios. Generally, if combustion is included, it is approximated using relatively simple one-step reaction mechanisms [39, 40] for liquid or gaseous fuels such as methane.

While solid fuel pyrolysis models [41-44] have been developed and incorporated into fire field models to simulate fire spread over flat solid fuel surfaces within compartments, it is difficult to use these pyrolysis models for complex mixtures of fuels such as may be found in aircraft cargo holds full of luggage. In most practical engineering calculations, the conventional handling of this difficulty is to use the volumetric heat source model. In this it is assumed that the total heat released from the fuel source is released within a prescribed volume and the heat release rate is provided from experimental data or empirical relations. In other words, the model assumes that the mass loss due to the fuel burning, and the ensuing chemical reaction between the combustible pyrolysis products of the mass loss processes and oxygen, only take place in the prescribed region and outside this region there is no chemical reaction. In practice it is difficult to estimate the size and location of the prescribed heat release region even though the size and location of the fuel source is generally known.

Furthermore, the combustible pyrolysis products released from the fire source may be transported outside the original region of the solid fuel and combustion may also occur outside of this region.

In these types of models, in addition to representing the heat release rate as a source term, it is also possible to treat the other fire products such as smoke, CO, etc. as an imposed time dependent volumetric source term. As this project is primarily concerned with predicting the impact of the water mist on the enclosure atmosphere, the volumetric release rate approach was adopted to represent the fire.

3.1 The Fire Submodel

The governing equations for all fluid variables can be expressed in the general form:

$$\frac{\partial \rho \phi}{\partial t} + \mathrm{div}(\rho \underline{U} \phi) = \mathrm{div}(\Gamma_\phi \nabla \phi) + S_\phi \qquad (1)$$

where S_ϕ is the source term and ϕ stands for any one of the following variables: the velocities *u, v, w* in the three co-ordinate directions, the enthalpy *h,* the turbulent kinetic energy *k,* its dissipation rate ε and other scalar product concentrations (i.e., CO_2, H_2O, CO, and O_2). For the continuity equation ϕ takes the value of one [19].

The FIREDASS fire submodel generates the sources of heat, smoke, and gaseous combustion products (CO_2, H_2O, CO, and O_2) representing the fire and adds them into the appropriate gas phase equations [4]. The heat source is added into the enthalpy equation; the smoke source is added as a concentration flux to a scalar equation; the gaseous combustion gases are modeled as simple mass fractions and an appropriate mass flux is added to these equations. In addition the combined mass flux from the combustion gases is added into the pressure correction (mass continuity) equation as a source of mass. It is assumed that the source terms all act in the same specified volume. When the CFD engine solves the

gas phase equations these sources are convected and diffused throughout the compartment. In this way the effect of the fire on the flows, temperatures etc. in the compartment is accounted for. As the fire submodel does not directly simulate combustion, accurately prescribed release rates, derived from experimental data are required.

The fire submodel allows all the parameters specifying the fire scenario to be entered via input files so that the user does not need to modify or recompile the software. Parameters specified via these input files include enclosure geometry, details of wall fluxes-temperatures, air leakage rates, and the release rates of the various fire products.

A range of methods are provided for handling solid wall boundary conditions. These include:

- fixed flux (including adiabatic);
- fixed temperature;
- imposed variable convective heat flux and imposed variable radiative heat flux;
- imposed variable temperature; and
- full boundary modeling using solid structures.

The fire source may be set at any arbitrary location and to posses any arbitrary volume within the geometry. The fire submodel fits this volume to the constraints of the grid. Alternatively the user may allow the fire submodel to vary the volume of the fire according to the Heskestad relation [45]. Here the horizontal cross sectional area of the fire is kept constant but the height is varied according to:

$$L = 0.23\dot{Q}_c^{2/5} - 1.02D \tag{2}$$

where L is the plume height (in m), $\dot{Q}_c$ is the convective heat flux generated by the fire (in kW) and D is the equivalent diameter of the surface area of the fire (in m). The area of the fire and its original height are specified in the input file. This height is taken as a minimum value. The height required according to the above formulation is calculated at each timestep. If it exceeds the original height then the number of cells included in the volume of the fire vertically is increased until the calculated height is just exceeded. The new heat source is uniformly distributed over this increased volume.

3.2 The Thermal Radiation Submodel

Thermal radiation is the dominant mode of heat transfer in compartment fires. The radiation submodel [7, 8, 31] simulates the generation of thermal radiation by the fire and its transport throughout the compartment. Absorption and scattering by the combustion gases, smoke, water-mist, and compartment surfaces are accounted for. Heat sources representing absorption from the radiation field

are passed to both the CFD engine for inclusion in the gas field calculations and the water-mist submodel for inclusion in the droplet temperature calculations. The radiation interaction with the water-mist phase will be the subject of a later publication [29] and is covered elsewhere [6, 8, 30] so it will not be discussed in this paper.

As a first approximation, the six-flux model is used to describe thermal radiation [25]. This model has already been successfully applied to a number of practical problems involving radiation [23, 38, 44]. The six radiation fluxes modeled are those in the positive and negative x, y and z directions. They are denoted by F^+, F^-, F^+, F^-, F^+, and F^- respectively. By defining $R_x = F^+ + F^-, R_y = F^+ + F^-, R_z = F^+ + F^-$ it is possible to derive the following second-order ordinary differential equation:

$$\frac{d}{ds}\left[\frac{1}{\alpha}\frac{d}{ds}R_\alpha\right] = S_\alpha ; \alpha = x, y, z \tag{3}$$

where $S_\alpha = R_\alpha(a+s) - 2a\sigma T^4 - s\,(R_x + R_y + R_z)/3$, a and s are the absorption and scattering coefficients respectively and σ is the Stefan-Boltzmann constant.

The primary attraction of this model is that it is easily incorporated into the finite volume scheme of the numerical solution procedure adopted by fire field models and is much less computationally intensive than other advanced radiation models such as the discrete transfer method [46]. This later point is of prime importance as the model, if it is to be used in an engineering context, must be as computationally efficient as possible.

At symmetry boundaries, the radiative heat flux is zero by definition. This is the default boundary condition in CFX 4.1 for all scalar transport equations. A perfectly-reflecting boundary may be created by setting the surface emissivity to zero. At non-reflecting boundaries, such as openings or free boundaries, the outgoing radiation leaves the calculation domain without reflection and only the incoming radiation needs to be prescribed. Thus, for example, the incoming flux at an inlet boundary may be defined as:

$$K_{in} = \varepsilon_g \sigma T_{in}^4 \tag{4}$$

where ε_g is the inlet gas emissivity and T_{in} is the inlet gas temperature. For a wall, if the net radiative wall heat flux is known, then S_α can simply be set equal to half of the prescribed wall heat flux. If the wall temperature is prescribed then the required radiative flux may be derived by considering the radiation flux leaving the wall. This consists of both the reflected and emitted radiation.

3.3 Fire-Radiation Coupling

The fire submodel adds the heat output from the fire to the gas phase enthalpy equation in the computational cells in the volume of the domain specified as being occupied by the fire (see equation 2). Consequently high temperatures are obtained

in this volume. The radiation equations include an energy term representing the addition to the radiation field of the black body radiation emitted by the hot gas. This energy source is the driving force for the radiation field. Since this source depends upon the fourth power of the gas temperature it is dominated by the contribution from the very hot gas in the computational cells containing the fire. In this way the radiation field is produced by the coupling of the fire and radiation submodels. Note that, as the FIREDASS model does not account for soot, it is assumed that the soot temperature is identical to the gas temperature. This is not strictly correct as the soot will generally be hotter than the gas.

4 VERIFICATION OF THE FIRE AND RADIATION SUBMODELS

The fire and radiation submodels have been validated against available experimental data in two stages. First, as each submodel was developed it was tested against experimental data. The submodels were then combined and the full model tested against more challenging experimental scenarios. For the tests of the component submodels a set of experimental data readily available in the fire literature, one commonly used for this purpose, that of Steckler et al. [47], was used. This data set consists of the results of a series of fire tests in a small well ventilated compartment. Predictions made by the separate fire and radiation submodels were compared with this experimental data set. The results generated were in good agreement with the experimental data and were consistent with predictions produced by other fire field models including PHOENICS and FLOW3D 2.3 [4, 7]. For the tests of the combined fire submodel, radiation submodel and CFD engine the experimental results obtained from fire tests conducted as part of the FIREDASS programme were used. These fire tests consisted of a systematic set conducted by SINTEF [3] and were designed and performed specifically for the purpose of generating data for the validation of these models.

4.1 The SINTEF Fire Trials

The SINTEF experiments were conducted with and without the presence of water mist. While these experiments were not conducted in an aircraft cargo hold mock-up, the fire scenarios were intended to resemble as far as possible the target application environments. The SINTEF trials were performed in a metal container equipped with a chimney to a low the combustion products to escape and a forced air supply to represent leakage into an aircraft cargo hold, arranged as shown in Figure 2. Instrumentation included (see Figure 3):

- 72 thermocouples to measure gas temperatures;
- 6 velocity probes to measure gas velocities;
- 3 total heat flux meters to measure the total heat flux to a target wall;

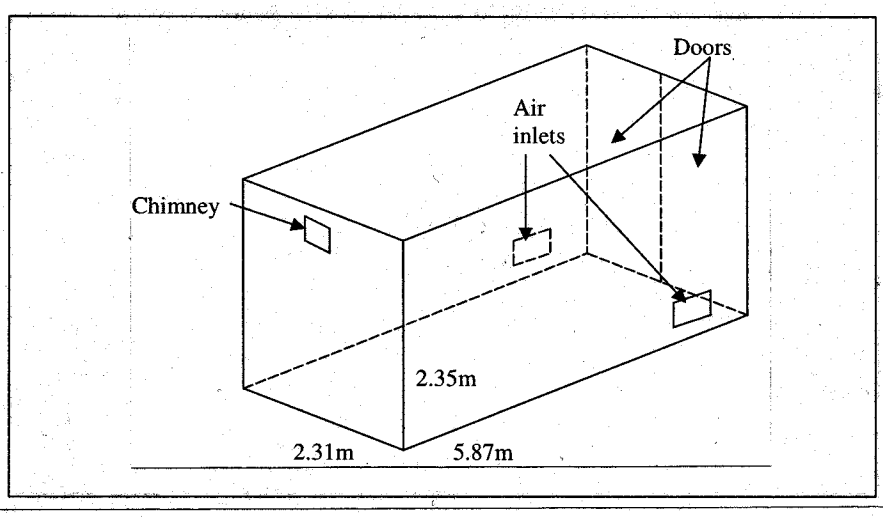

Figure 2. Schematic of SINTEF test compartment.

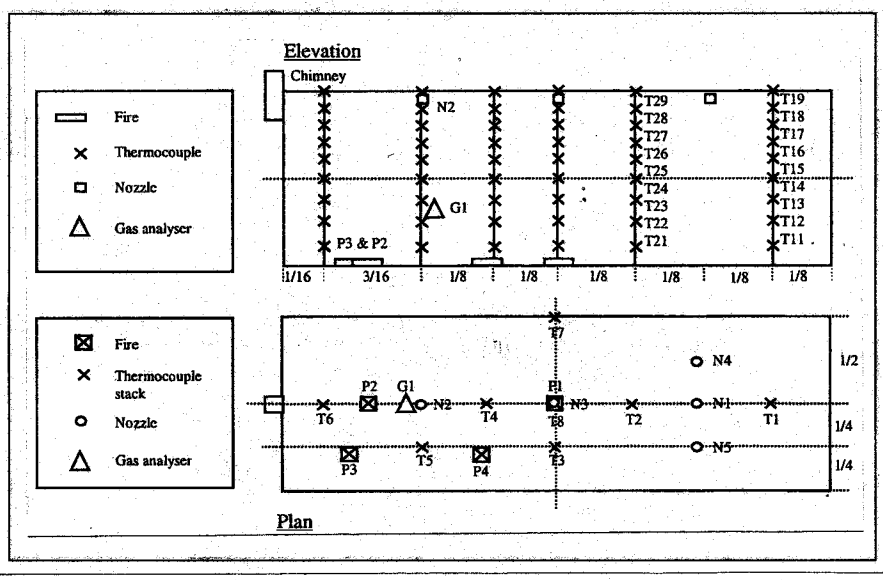

Figure 3. Diagram showing instrumentation of SINTEF test compartment.

- 3 radiative heat flux meters to measure the radiative heat flux to a target wall.

In addition to the above, the following measurements were also made:

- concentrations of O_2, CO_2, CO in the chimney and centrally in the compartment (G1);
- water vapor concentration in the chimney and centrally in the compartment (G1);
- particle (soot) concentration in the chimney;
- wall temperature at two locations;
- pressure in the compartment.

A total of 35 experiments were performed involving different fire types, fire locations, numbers of obstacles, and numbers of nozzles. The fire types implemented consisted of gas burners, cardboard boxes, and kerosene pool fires. The experiments were all simulated using the FIREDASS numerical model and the predicted and experimental results compared [9].

4.2 Comparison of FIREDASS Numerical Predications with SINTEF Experimental Results

Due to space limitations, it is not possible to present all of the numerical predictions for these experiments. As a result, only a selection of the results will be presented here; interested readers can find the full results presented in the project report [9]. In this paper comparisons will be presented for the gas and smoke concentrations in the chimney, for the gas and smoke concentrations in the center of the room at location G1 (see Figure 3) and for the temperature at four representative thermocouple locations (see Figure 3), namely:

- T12—near the floor in the vicinity of the compartment doors;
- T18—in the same thermocouple stack as T12 but just below the ceiling;
- T58—just below the ceiling between fire positions P3 and P4;
- T36—located centrally and at approximately three-quarter height.

These comparisons will be presented for three different fire types. These are as follows:

- experiment 02HS utilized a propane gas burner;
- experiment 05PM utilized a small kerosene pool;
- experiment 06BXB utilized a line of three cardboard boxes.

In all three experiments the fire was located at position P2 (see Figure 3) and there were no obstacles in the compartment. In the 02HS case, gas was supplied to the burner for a predetermined period of time, after which the supply ceased. For the 05PM and 06BXB cases, the fuel or boxes were lit and then allowed to burn

until self-extinguishment occurred, either through consumption of all of the oxygen in the compartment or all of the fuel.

In all three simulations the following boundary conditions were imposed:

- all compartment surfaces (including the floor and ceiling) were modeled as isothermal surfaces at 288 K;
- for the gas velocities the non-slip condition was applied on all surfaces;
- the k-ε turbulence model was used with the standard wall functions;
- with the exception of the chimney, all boundaries were sealed allowing zero mass transfer;
- the chimney was treated as a zero pressure boundary with ambient conditions outside, so in the event of reverse flow, i.e., air being drawn into the compartment, fresh air was entrained;
- in the radiation model all compartment surfaces (including the floor and ceiling) were assumed to have an emissivity of 0.9 and a temperature of 288 K.

02HS—THE PROPANE BURNER CASE

In this experiment the fire source consisted of a propane burner which had a fixed supply of gas. The burner was allowed to burn for a predetermined period of time before the gas supply was terminated. All measurements were taken for the duration of the burn and for 15 minutes after the gas supply was terminated.

As the experimental setup was symmetrical only half the compartment was simulated in order to save computational time. The mesh used had 39 cells along the long axis, 22 vertically, and 13 in the half width of the compartment, a total of 11,154 cells. Cells were concentrated in the vicinity of the surfaces and of the fire. Figure 4 shows the mesh in the vertical plane along the long central axis of the compartment, the symmetry plane.

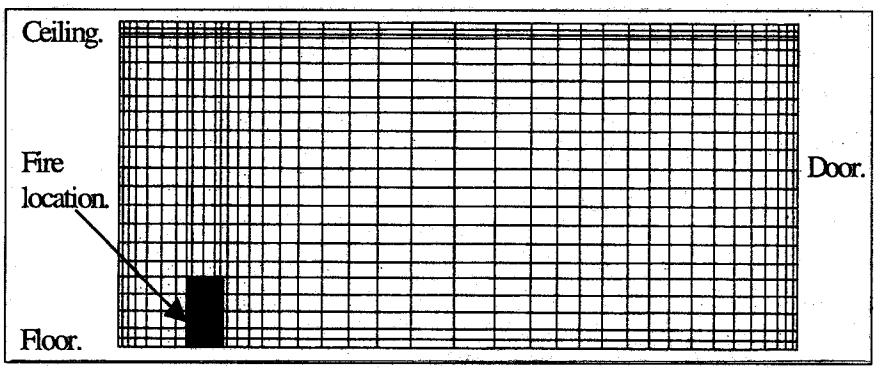

Figure 4. Mesh on the symmetry plane for 02HS problem.

In the experiment the fire started at t = 24s, so this is the point at which the simulation was begun. Simulation time therefore ran from t = 24s to t = 724s, i.e., a total of 700s of real time was simulated. This required 35 hours of CPU time on a DEC Alpha 466MHz processor.

As described in section 3, the fire was represented as a volumetric source of heat, CO_2, H_2O, and a sink for O_2. As the simulation uses a Cartesian grid the volume used to contain the release rate sources was cuboid in shape with a square horizontal cross section whose area was equal to the area of the gas burner (~0.09 m^2). Its flame height was determined automatically by the fire submodel using the Heskestad formulation [45]. Note that as the heat release rate of the fire was constant throughout the simulation, the height also remained constant (~1.5 m). All sources were distributed uniformly throughout the volume.

The heat release rate (HRR) for the gas burner was determined from the propane supply rate and the heat of combustion of propane with an assumed average combustion efficiency of 80 percent. This produced a uniform HRR of 117 kW for the duration of the burn, i.e., from 48s to 421s. The HRR ramped to this value between 24 and 48 seconds and back to zero between 421 and 429 seconds.

No data was available for the production rates of the other combustion products. The production rates of the CO_2 and the H_2O and the consumption rate of the O_2 were therefore calculated stoichiometrically from the propane supply rate and then scaled by 0.8 like the HRR to represent a reduced combustion efficiency. This gave production rates of 0.00764 kg/s for the CO_2, 0.00416 kg/s for the H_2O, and –0.0088 kg/s for the O_2. It was assumed that neither CO nor smoke were produced.

In reality the combustion efficiency is not constant but varies throughout the experiment. The efficiency is likely to be large at the start of the fire and then tend to decrease as the oxygen within the compartment is consumed. Representing the combustion efficiency as an average value is therefore a crude approximation. This has implications for all the release rates used in the model. For the combustion products, CO_2 and water vapor, the production rates will be over-predicted as will be the consumption rate of oxygen. It was also assumed that generation rates for the products of incomplete combustion, i.e., CO and soot, are zero. It was noted from visual observation however that as the experiment progressed small quantities of smoke started to be produced.

The main results for this simulation are presented in Figures 5 to 11. These show comparisons between the experimental results and the model predictions for various parameters at various locations within the compartment as a function of time.

Figures 5 to 7 depict the temperature distribution at three locations. Figure 5 is thermocouple T12 (located on the long symmetry axis, toward the front of the compartment and near the floor, see Figure 3), Figure 6 is thermocouple T18 (same thermocouple tree as T12 but located just below the ceiling), and Figure 7 is thermocouple T36 (located on the short symmetry axis, half way between the compartment centre and the wall, approximately 1.75 m above the floor, see

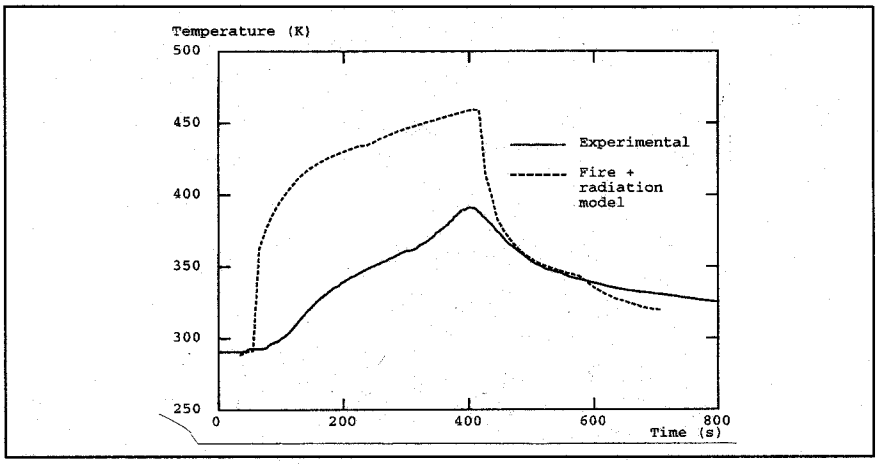

Figure 5. 02HS case. Predicted and measured temperature variation at T12 (near floor and doors).

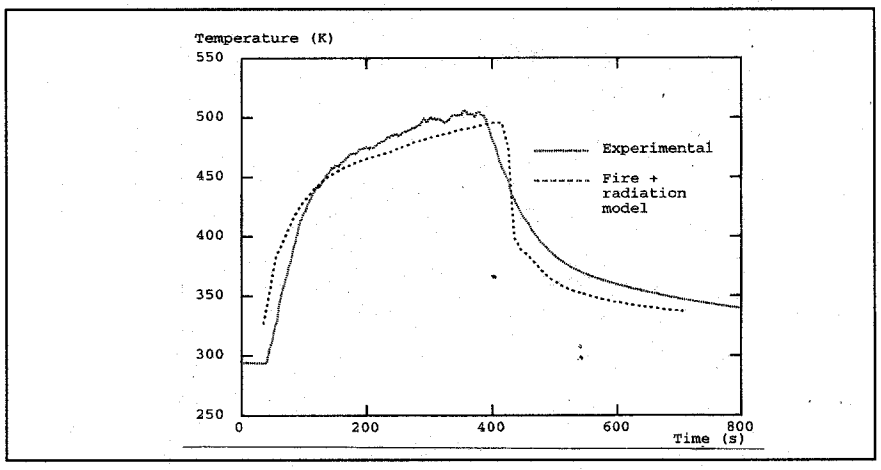

Figure 6. 02HS case. Predicted and measured temperature variation at T18 (near ceiling and doors).

Figure 3). It can be seen that, in the experiment, once the fire has started, temperatures in the upper part of the compartment rise rapidly before starting to level out as an equilibrium is reached between the heat sourced by the fire and the heat lost through the walls and chimney. An equilibrium would be possible in this case as the fire has a steady heat release rate. When the fire is extinguished the temperatures fall rapidly again due to continued heat loss through walls and

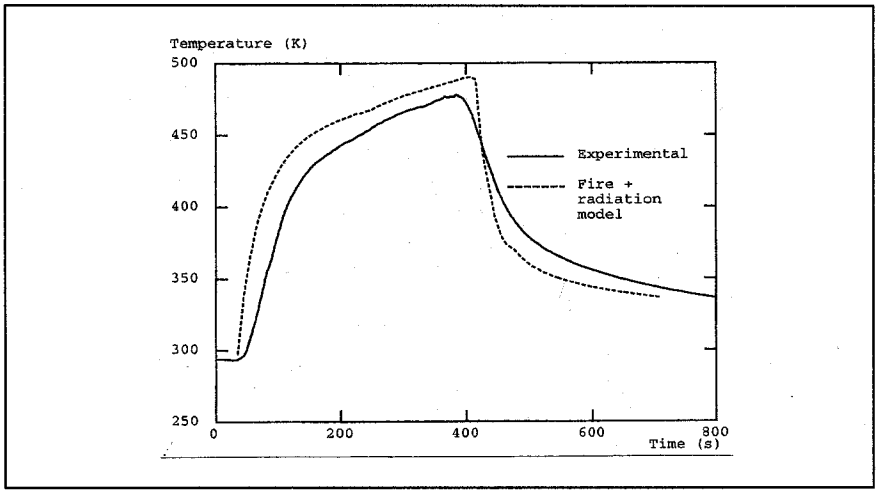

Figure 7. 02HS case. Predicted and measured temperature variation at T36 (3/4 height and central).

chimney and the flow of cold fresh air in at floor level through the inlets. Temperatures lower in the compartment rise more slowly but are still rising when the fire is extinguished. This is due to the hot layer continuing to deepen as the fire burns.

As can be seen from Figures 6 and 7, there is quite good agreement between measured and predicted temperatures high up in the compartment, the temperature prediction near the ceiling, Figure 6, providing the best match to the experimental results. From the point of view of creating a ceiling based, temperature operated, detection system this is an important result. The growth and decay portions of the temperature curves and the peak temperatures are well captured by the numerical predictions. However, temperatures near the floor are severely over-predicted. Here we find that the predicted temperature growth is much more rapid than that measured and that the peak temperature is over-predicted by 17 percent. The exact reason for this discrepancy has not yet been determined and is the subject of continuing research. It is likely however that it is due to the use of approximate thermal wall boundary conditions, the assumption of zero smoke production and the interaction of these factors with the radiation field.

In discussing the comparison between measured and predicted temperatures it should be noted that there is an uncertainty of "several degrees" [3] in the temperatures measured by the thermocouples.

Figures 8 to 11 compare predicted and measured concentrations for the combustion gases. Figure 8 depicts the CO_2 concentration in the chimney, while

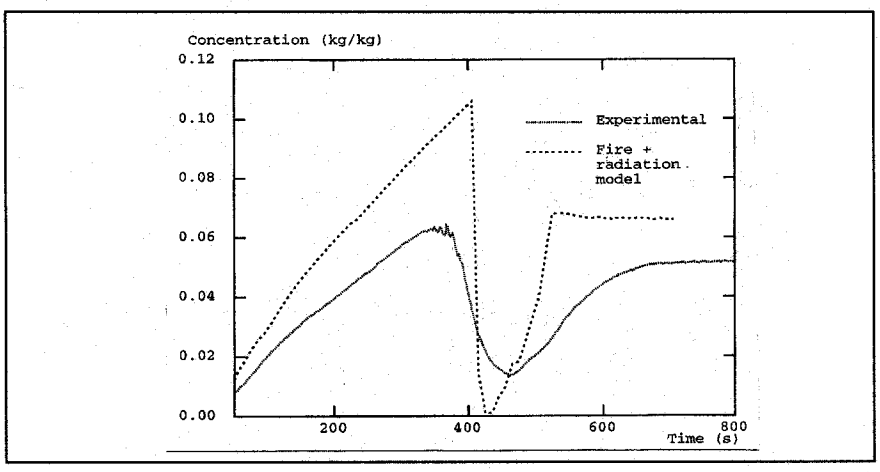

Figure 8. 02HS case. Predicted and measured CO_2 variation at the chimney.

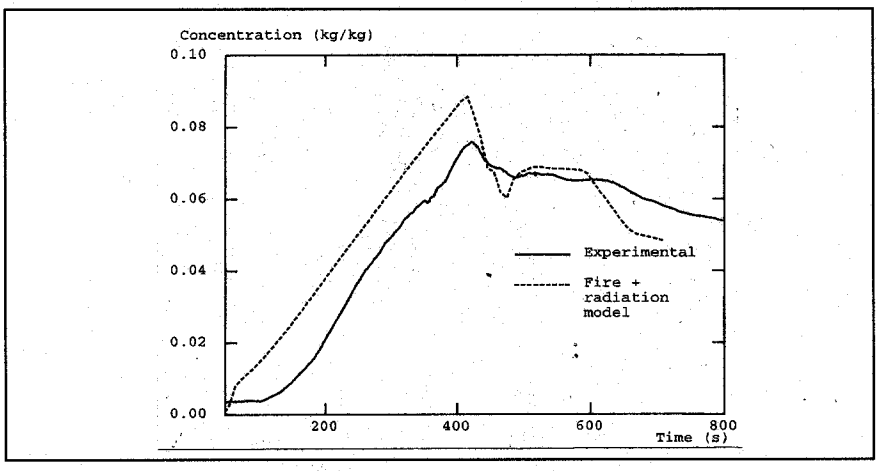

Figure 9. 02HS case. Predicted and measured CO_2 variation in the room at location G1.

Figures 9 to 11 depict the CO_2, O_2, and H_2O concentrations at G1, a point located on the long symmetry axis half way between the compartment center and the chimney wall, approximately 0.59 m above the floor. In this case CO was not considered as the values measured were very small and hence involved large uncertainties.

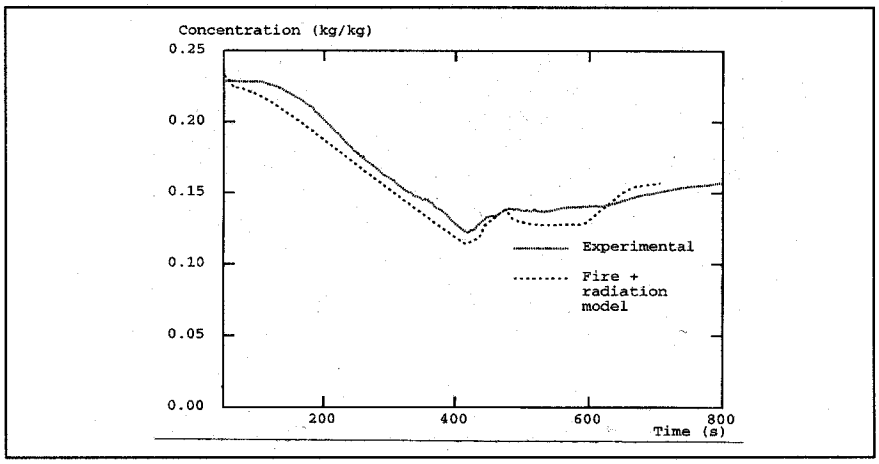

Figure 10. 02HS case. Predicted and measured O_2 variation in the room at location G1.

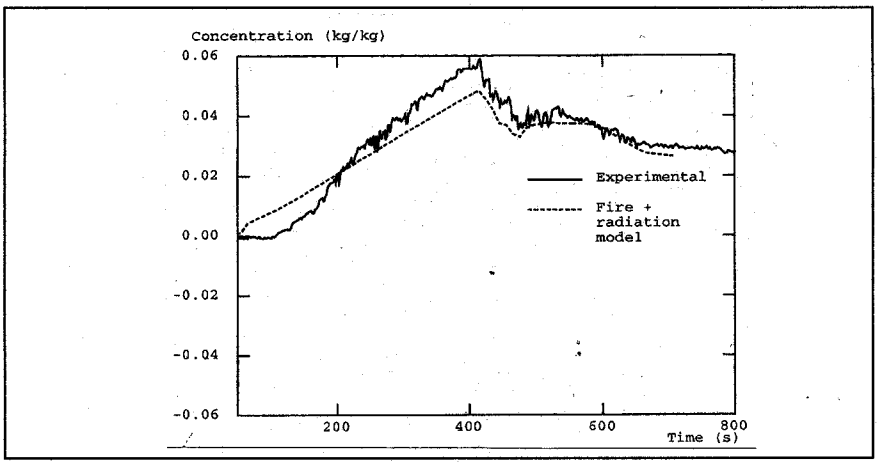

Figure 11. 02HS case. Predicted and measured H_2O variation in the room at location G1.

From Figure 9 it can be seen that as the fire bums the CO_2 it produces builds up in the compartment, the concentration increasing from less than 1 percent to over 7 percent. When the fire is extinguished, at 420s, the concentration immediately starts to drop. This is as would be expected since the sampling point is low down in the compartment and the compartment is being supplied with cold fresh air at floor level. After the fire has been extinguished this flushes all the combustion products out of the compartment and returns gas concentrations to ambient levels. As can be

seen from the graph this process occurs slowly due to the volume of the compartment and the turbulent mixing which takes place, combustion products from high in the compartment being mixed with the fresh air entering the compartment lower down.

From Figure 8 it can be seen that the increase in the CO_2 concentration in the compartment, Figure 9, is matched by a corresponding increase in the concentration of CO_2 in the flow through the chimney. Since this flow is drawn from high in the compartment and away from the fire the combustion products have had time to mix with the gas in the bulk of the compartment so the CO_2 concentration is slightly lower than at the sampling point in the compartment, which is near the fire. However, as the fire starts to die due to oxygen depletion and is then extinguished the temperature in the compartment starts to drop, see Figure 6. As the air in the compartment cools it contracts, resulting in the flow through the chimney reversing. Since the chimney is long, mixing between fresh air entering and hot buoyant gases trying to escape occurs. This results in the measured CO_2 concentration in the chimney dropping slowly toward ambient levels as the chimney is cleared of combustion products. Once the compartment stops cooling the flow returns to normal due to the inflow of fresh air through the vents creating a flow out through the chimney. The CO_2 concentration measured in the chimney therefore returns to the value in the compartment and then shows the same slow decline to ambient values as in the compartment.

Simulated results show excellent qualitative agreement with this behavior. The main difference occurs due to the fact that in the simulation the chimney is modeled as an exit and not as a long pipe. Consequently when the flow reverses the predicted CO_2 concentration immediately drops to ambient values. The quantitative agreement is also quite good though there does seem to be a systematic over-prediction. This suggests that there may be a problem with the source terms, which it will be recalled were assumed and not measured.

As can be seen from Figure 11 the H_2O concentration in the compartment shows the same behavior as the CO_2, that is a steady rise up to 420 s when the fire is extinguished followed by a slow return to ambient values as the combustion products are flushed out of the compartment. As before, the simulation results show excellent qualitative agreement, accurately capturing the behavior of the system. The quantitative agreement is also quite good though there may be a tendency to under-predict the concentration. Again it should be recalled that these predictions are based upon assumed and not measured production rates.

Figure 10 depicts the O_2 concentration in the compartment. Here the concentration falls steadily as the fire progresses as the O_2 is being consumed. As with the other combustion products, when the fire is extinguished at 420 s the concentration starts to return to ambient values as the compartment is flushed with clean air.

The concentrations of CO_2, O_2, and H_2O were obtained by drawing the air out of the compartment down suction lines to gas analyzers. For the CO_2 and O_2 measurements the gas analyzer has a nominal accuracy of ± 1 percent. It is likely however that the experimental error is in fact substantially greater than this due to the length of the suction lines which had to be used and the time taken for the sample to get to the analyzer (5 m with a sample to result time of 38 s in the case of the samples from the center of the compartment). For the H_2O the measurements were based upon a technique involving heating the sample to a high temperature (around 150°C) and then measuring its relative humidity and temperature and using these to calculate the absolute humidity. The exact experimental error is hard to quantify but is likely to be substantial both as a consequence of the need to use long suction lines to obtain the sample and the difficulty of making the actual measurements. When comparing the experimental and theoretical results therefore, it should be remembered that the experimental results have considerable uncertainty associated with them.

05PM—THE KEROSENE POOL FIRE CASE

The fire source in this experiment consisted of a 0.5 m square tray of kerosene. The kerosene was supplied from a reservoir at a rate adjusted to keep a constant liquid level in the tray with the overflow led to a second reservoir. The pool was ignited and allowed to burn until it self-extinguished through oxygen starvation. This required approximately seven minutes. The data was recorded throughout the burn and for approximately 10 minutes afterwards.

For the simulation essentially the same mesh was used as for the 02HS case, only the number of cells along the long axis was increased to provide a better resolution of the physically larger fire. The mesh was 41 by 22 by 13, a total of 12,584 cells. In the experiment the fire started at $t = 50$ s, so this is the point at which the simulation was begun. Simulation time therefore ran from $t = 50$ s to $t = 895$ s, i.e., a total of 845 s of real time was simulated. This required 34 hours of CPU time on a DEC Alpha 400MHz processor.

As described in section 3 and in the 02HS case, the fire was represented as a volumetric source of heat, CO_2, H_2O, and sink of O_2. For this case, sources of CO and smoke were also included. As before the sources were imposed in a volume determined using the Heskestad formulation.

The nature of the prescribed heat source was determined in the following way. The reservoir supplying the kerosene to the fire and the reservoir collecting the over-spill were both mounted on scales and weighed continuously during the experiment. The difference between the quantity supplied and the quantity collected, after allowing for the thermal expansion in the tray and the time delay between leaving the supply reservoir and arriving in the collection reservoir, was taken to be the quantity of oil evaporated. To get the perfect combustion

efficiency heat release rate it was assumed that 100 percent of this was burned and that the oil had a constant net heat of combustion. This allowed the heat release rate of the fire to be calculated as a function of time. As with the 02HS case no direct measurements of the sources of CO_2, H_2O, and O_2 were available so their production-consumption rates were calculated stoichiometrically from the amount of kerosene consumed. The source terms therefore become multiples of the heat release rate.

Also as with the 02HS case the simulations were run with all sources multiplied by a scaling factor of 0.8 to represent an average real combustion efficiency of 80 percent over the course of the burn. The resultant peak rates used were heat, 80.8 kW, oxygen, –0.006 kg/s, water vapor, 0.0025 kg/s and CO_2, 0.0052 kg/s and the resultant HRR curve is shown in Figure 12.

The CO and smoke sources were determined by using standard tables of the yields of combustion products for well ventilated fires [48]. These give the source of CO and smoke in grams per gram of kerosene burned, which was known. When the usual 80 percent efficiency factor was included this resulted in peak production rates of 7.7×10^{-5} kg/s for the smoke and 2.2×10^{-5} kg/s for the CO.

The main results for this simulation are presented in Figures 13 to 21. These show comparisons between the experimental results and the model predictions for various parameters at various locations within the compartment as a function of time.

Figures 13 to 15 depict the temperature distribution at the same three locations as used in the previous case, i.e., Figure 13 is at thermocouple T12, Figure 14 is at thermocouple T18, and Figure 15 is at thermocouple T36. It can be seen that the temperature histories are similar to those in the 02HS case, though here the curves

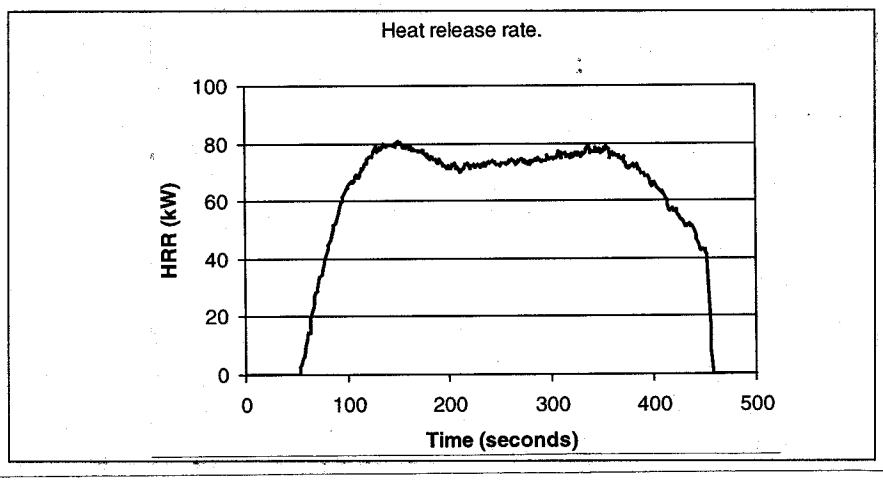

Figure 12. Heat release rate for kerosene pool fire.

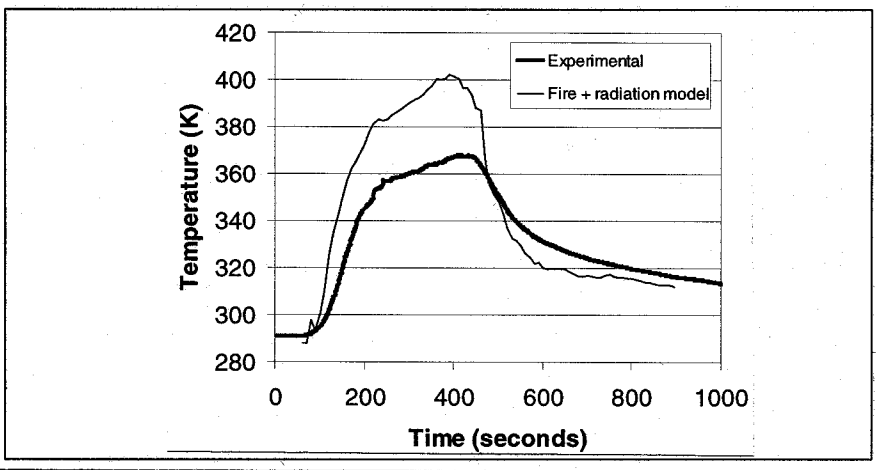

Figure 13. 05PM case. Predicted and measured temperature variation at T12 (near floor and doors).

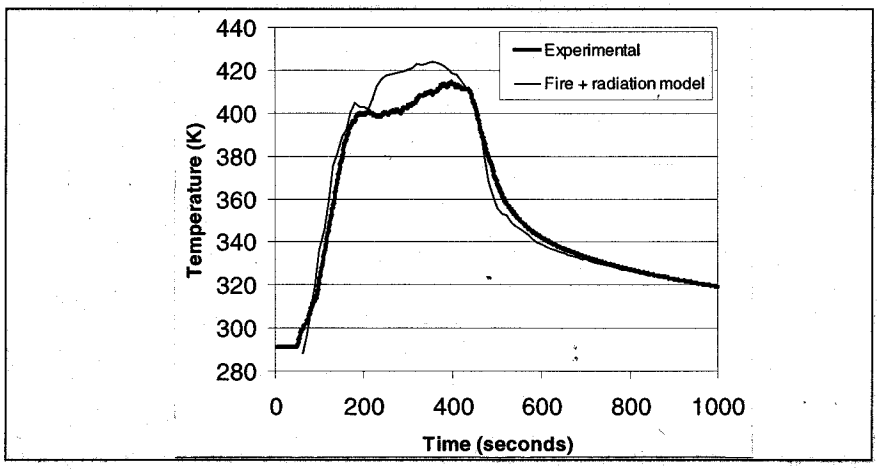

Figure 14. 05PM case. Predicted and measured temperature variation at T18 (near ceiling and doors).

are flatter once the initial rapid increase is over. This is because of the slight fall off in the HRR after its peak is reached. This will combine with the increased heat losses through the compartment boundaries to significantly slow any further increase in the temperature in the compartment.

As in the gas burner (02HS) case, there is quite good agreement between measured and predicted temperatures high up in the compartment. The shape of

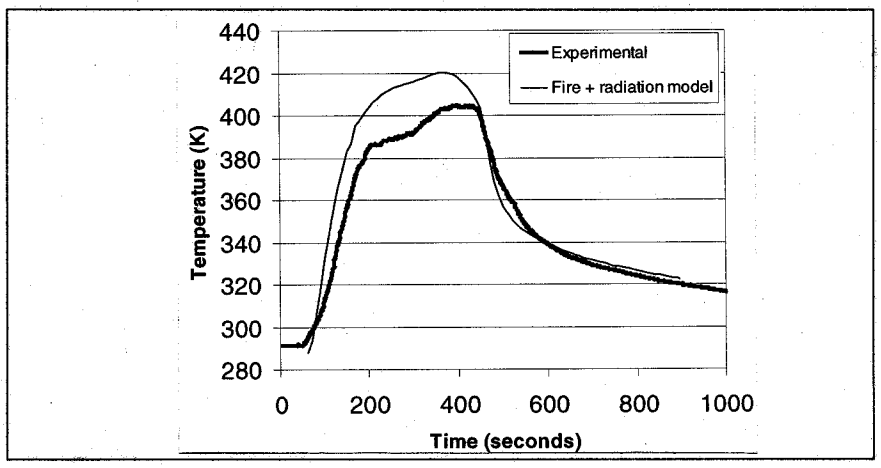

Figure 15. 05PM case. Predicted and measured temperature variation at T36 (3/4 height and central).

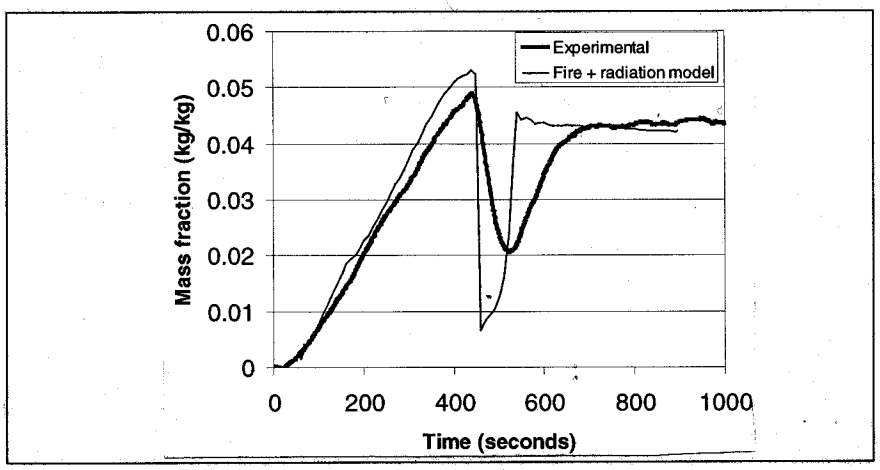

Figure 16. 05PM case. Predicted and measured CO_2 variation at the chimney.

these temperature distributions corresponds to the heat release rate curve in Figure 12. The growth and decay portions of the temperature curves and the peak temperatures are well captured by the numerical predictions. However, once again, temperatures near the floor are over-predicted. Near the floor we find that the growth of the predicted temperature is more rapid than that measured and that the peak temperature is over-predicted by some 9 percent. Similarly to the 02HS case, the crude thermal boundary conditions and the approximate smoke release

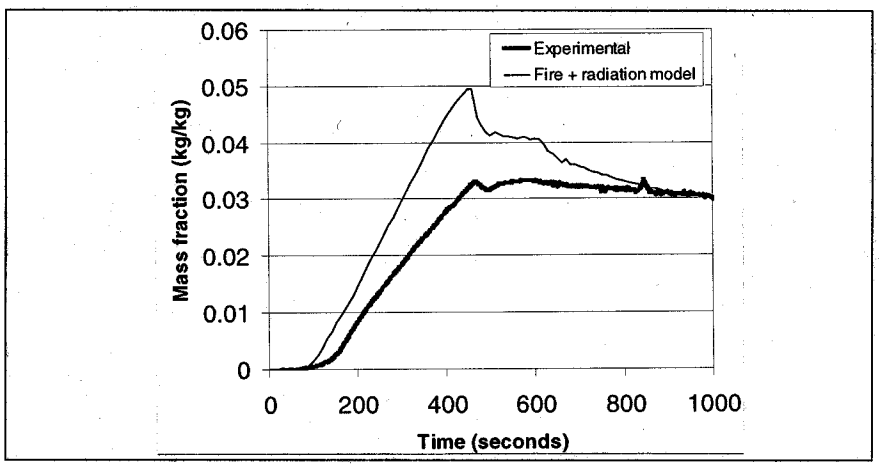

Figure 17. 05PM case. Predicted and measured CO_2 variation at room location G1.

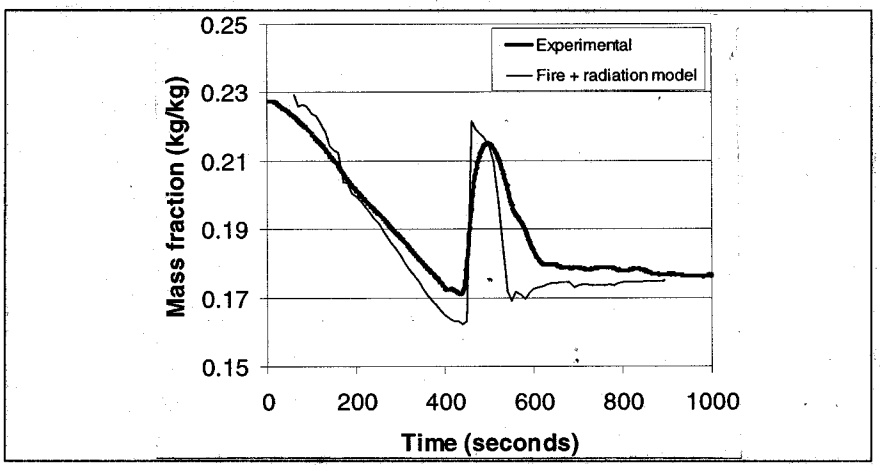

Figure 18. 05PM case. Predicted and measured O_2 variation at the chimney.

rates are thought to contribute to these discrepancies. In particular, while in this case smoke has been included, the source used assumed a well ventilated fire. In reality, as the fire proceeded and became under ventilated, the rate of smoke production per gram of fuel consumed will have risen.

Figures 16 to 19 compare predicted and measured concentrations for CO_2 and O_2 in the chimney and at location G1.

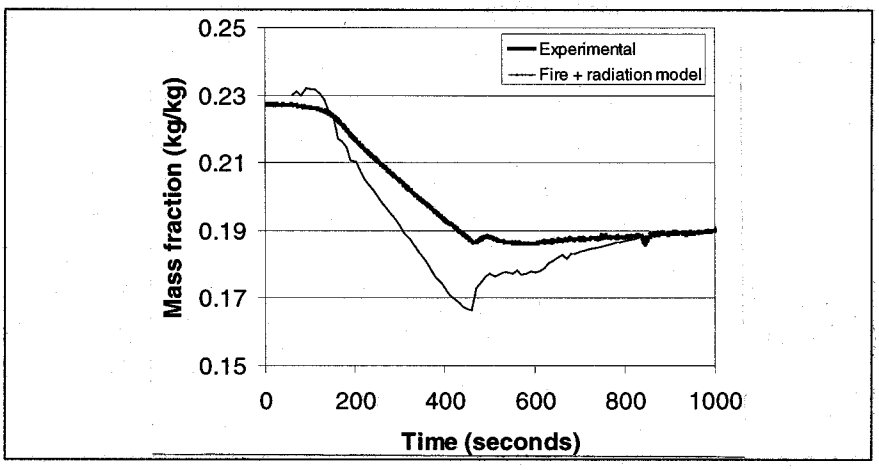

Figure 19. 05PM case. Predicted and measured O_2 variation at room location G1.

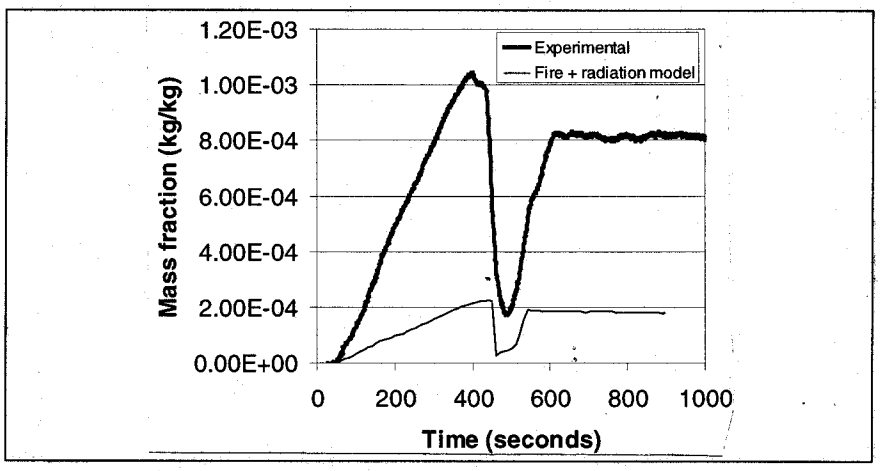

Figure 20. 05PM case. Predicted and measured CO variation at the chimney.

The behavior here is qualitatively the same as with the gas burner test, see the discussion in the previous section. There is the same build up in CO_2 and decline in O_2 as the fire progresses, the same reverse flow back in through the chimney when the compartment starts to cool after the fire self extinguishes and the same slow return to normal values as the compartment is flushed with clean air.

It can be seen that the numerical predictions for the CO_2 and O_2 concentrations at the chimney (Figures 16 and 18) are in good qualitative and quantitative

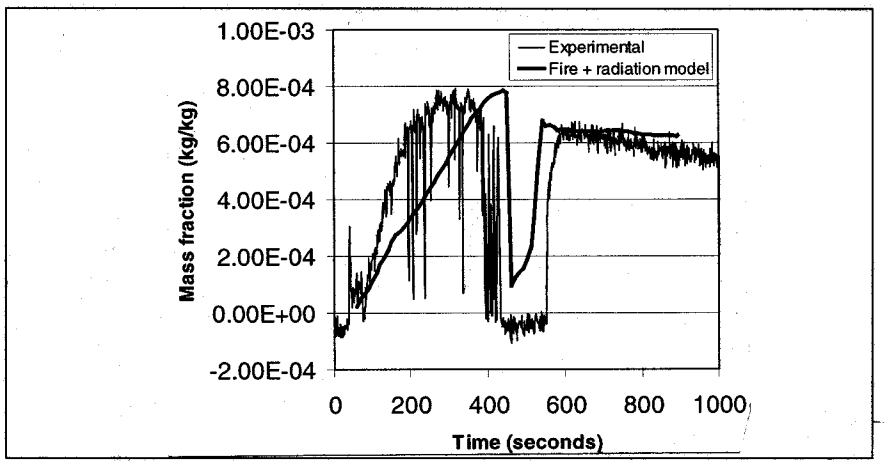

Figure 21. 05PM case. Predicted and measured smoke variation at the chimney.

agreement with the experimental values. At the internal gas analyzer location however, while the predictions are in good qualitative agreement with the experimental values, the model tends to over-predict the amount of CO_2 and under-predict the amount of O_2 present (Figures 17 and 19). The predicted values do however tend to the experimental values with time. It is likely that this discrepancy is due to the assumption of a constant combustion efficiency when in reality it will have varied during the course of the fire.

Figures 20 and 21 compare predicted and measured concentrations of CO and smoke in the chimney. The same behavior can be seen as for the other combustion products and in the 02HS case. That is, the concentration of combustion products increases as the fire bums, drops to ambient when the reverse flow through the chimney occurs and then increases again before slowly declining toward ambient values as the compartment is flushed.

The prediction of the smoke concentration is in good qualitative agreement with the experimental results. It is perhaps not surprising that there is a discrepancy in the level of quantitative agreement as the smoke concentration measurement is prone to error. The level of CO in the chimney however is severely under-predicted, though the qualitative agreement is good. The explanation for this under-prediction of CO in the chimney (and over-prediction of temperature and CO_2 within the compartment) lies in the nature of the combustion processes occurring within the compartment. The fire within the compartment is ventilation controlled and as such does not bum as efficiently as a free burning pool fire. The release rates imposed on the calculations however are essentially derived from free burning pool fires scaled uniformly by a factor of 0.8 across time and also across

all species. This is only an approximation however as the efficiency will have varied with time. It will also have varied across species. In particular, the rate of production of CO will increase and not decrease as the fire becomes oxygen depleted. Since no data was available to determine how much this increase was or how it varied with time the CO production rate had the same scaling factor applied as the other sources for consistency, i.e., 0.8. From Figure 20 it can be seen that an average scaling factor of around 5 may have been more appropriate for the CO.

06BXB—THE 3 BOX FIRE CASE

The fire source in this experiment consisted of three cardboard boxes measuring 0.5 m by 0.5 m by 0.5 m arranged in a row. They were filled with shredded paper, ignited and allowed to burn out. This required approximately three minutes. The data was recorded throughout the burn and for approximately 10 minutes afterwards.

To simulate the problem the same mesh was used as for the 05PM case. The model was run for 885 s, starting at 100 s into the experiment. This required 48 hours of CPU time on a DEC Alpha 466MHz processor.

As with the pool fire case the fire was represented as a volumetric source of heat, CO_2, H_2O, CO and smoke and sink of O_2. The heat release rate was determined by SINTEF using the Oxygen Depletion Technique. The resultant curve is shown in Figure 22, the maximum heat release rate achieved was 405 kW. Since this HRR was determined from the oxygen consumed rather than the fuel used it was not scaled as in the previous simulations to allow for efficiency. The

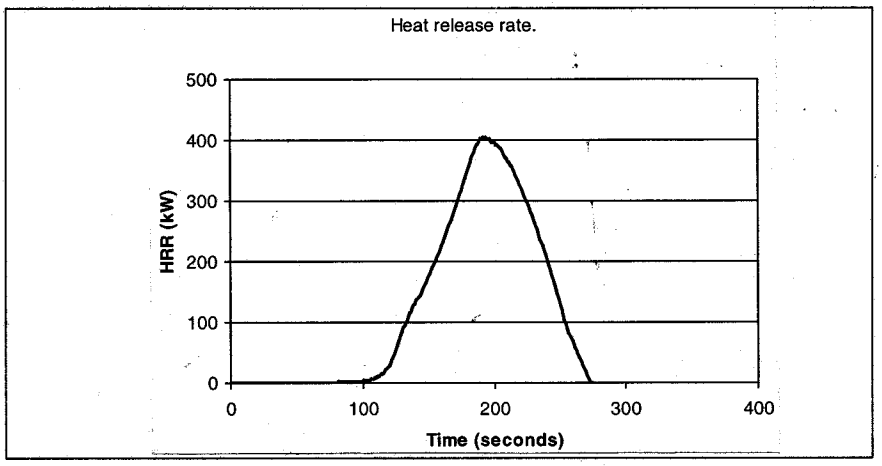

Figure 22. Heat release rate for three box fire.

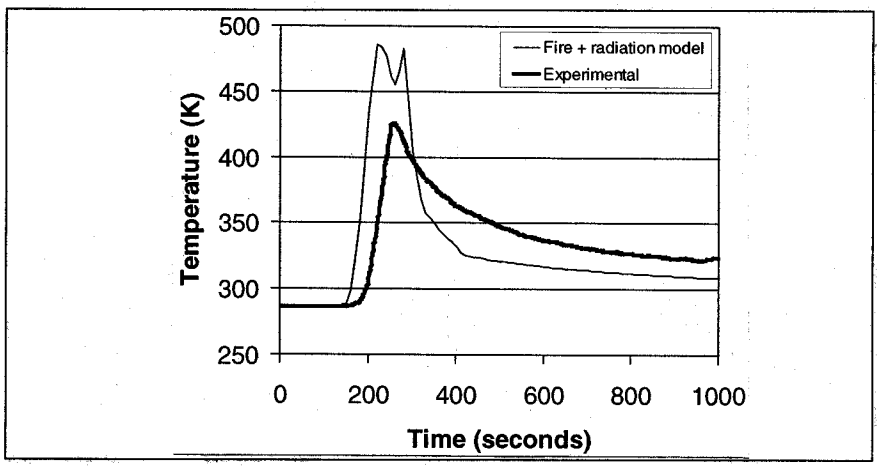

Figure 23. 06BXB case. Predicted and measured temperature variation at T12 (near floor and doors).

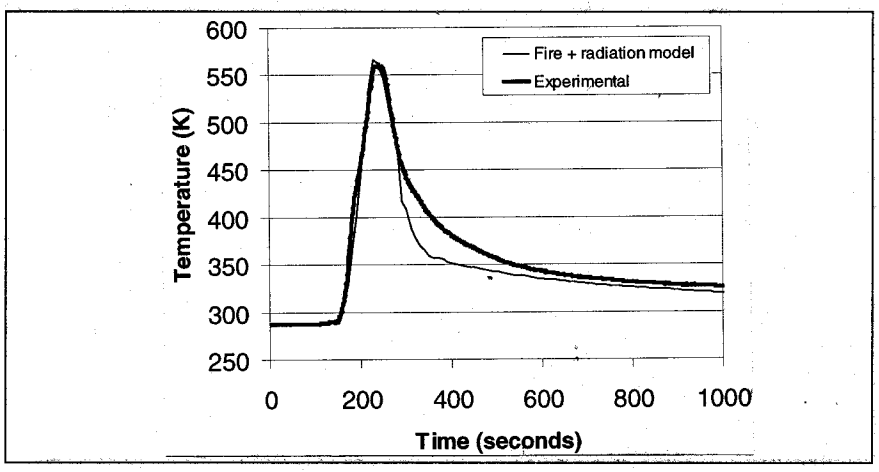

Figure 24. 06BXB case. Predicted and measured temperature variation at T18 (near ceiling and doors).

CO_2, H_2O, and O_2 production/consumption rates were determined, as before, by assuming stoichiometric consumption of cellulose. This results in maximum rates of 0.0181 kg/s of CO_2, 0.0657 kg/s of H_2O and –0.0372 kg/s of O_2. The production rates of CO and smoke are discussed later.

The main results for this simulation are presented in Figures 23 to 31. These show comparisons between the experimental results and the model predictions for

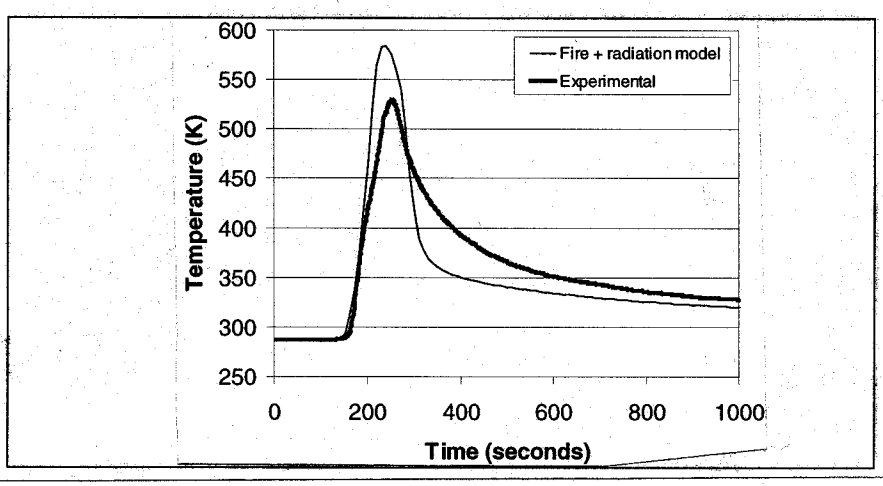

Figure 25. 06BXB case. Predicted and measured temperature variation at T36 (3/4 height and central).

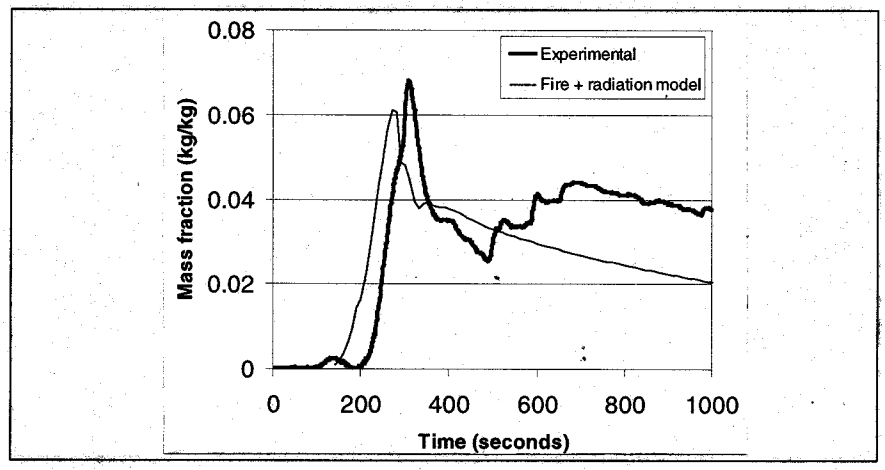

Figure 26. 06BXB case. Predicted and measured CO_2 variation at room location G1.

various parameters at various locations within the compartment as a function of time.

Figures 23 to 25 depict the temperature distribution at the same three locations used in the previous cases, i.e., Figure 23 is at thermocouple T12, Figure 24 is at thermocouple T18, and Figure 25 is at thermocouple T36. As the HRR curve is strongly peaked the temperatures in the compartment follow a similar trend—a

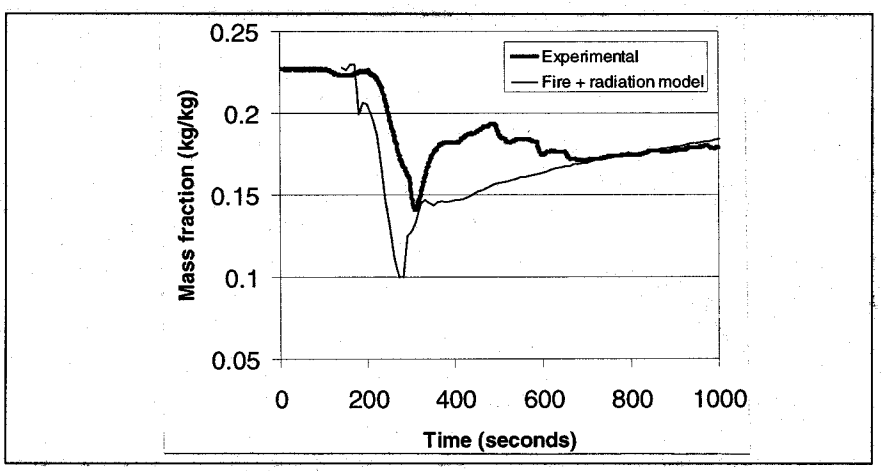

Figure 27. 06BXB case. Predicted and measured O_2 variation at room location G1.

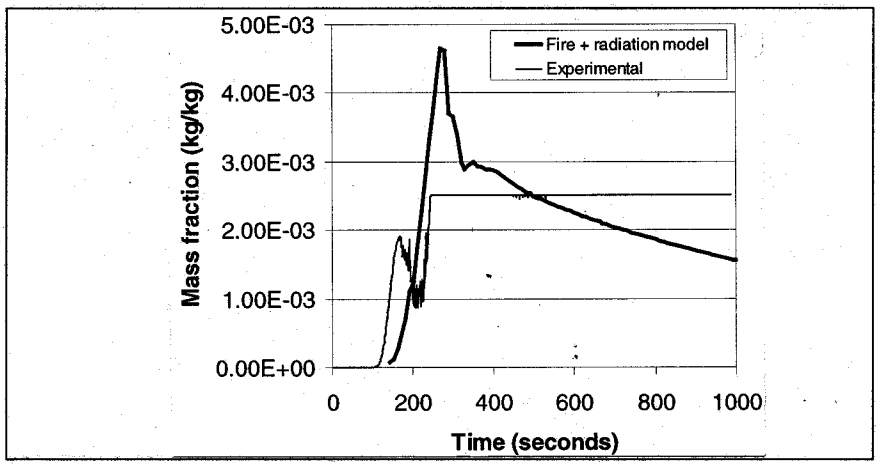

Figure 28. 06BXB case. Predicted and measured CO variation at room location G1.

rapid rise to a high temperature followed by a slower decay as the fire self-extinguishes and the compartment starts to cool.

As in the previous two cases, there is quite good agreement between measured and predicted temperatures high up in the compartment. The growth and decay portions of the temperature curves and the peak temperatures are well captured by the numerical predictions. However once again, temperatures near the floor are

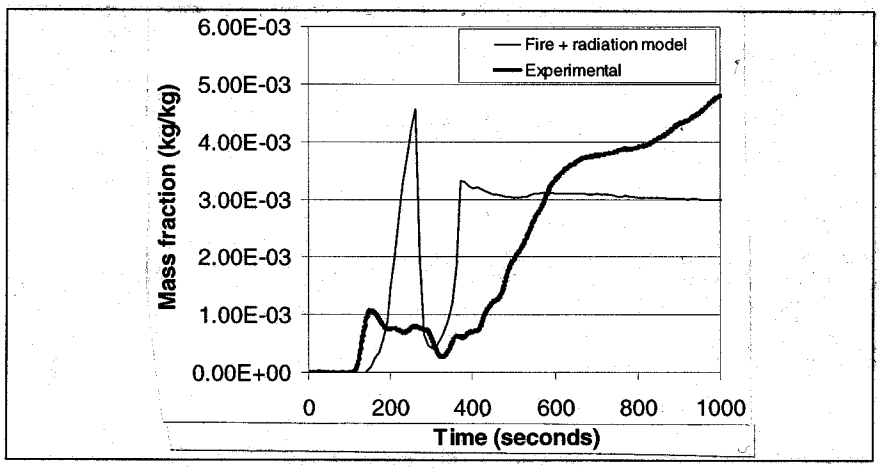

Figure 29. 06BXB case. Predicted and measured CO variation at the chimney.

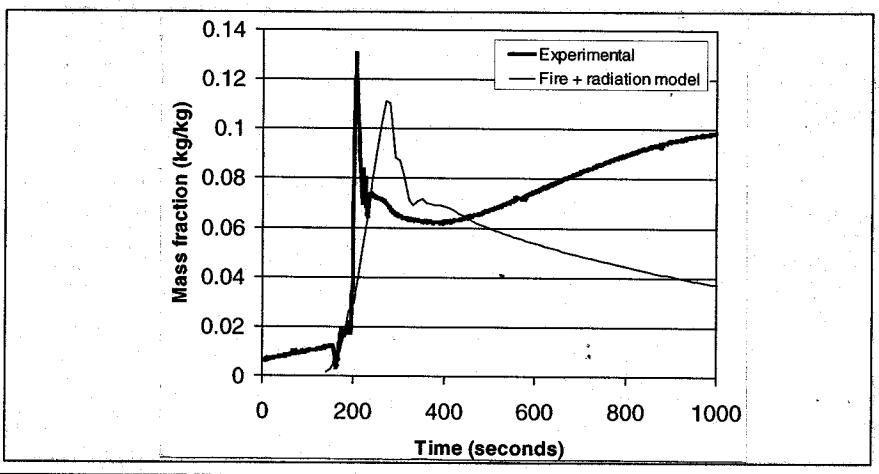

Figure 30. 06BXB case. Predicted and measured water vapor variation at room location G1.

over-predicted. Here we find that the growth rate of the predicted temperature is similar to that of the measured temperature but that the peak temperature is over-predicted by 14 percent. The main sources for this discrepancy are as explained previously for the 02HS and 05PM cases.

Figures 26 to 31 compare predicted and measured values for the combustion products. It can be seen from the experimental results that, as before, there is a

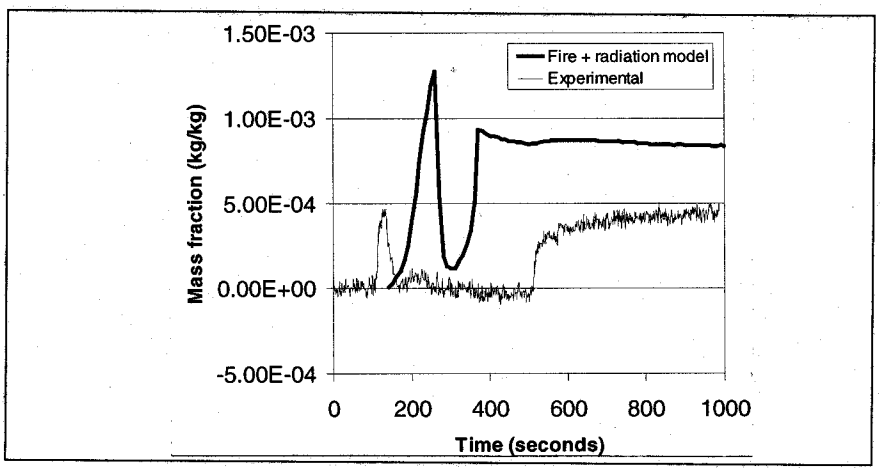

Figure 31. 06BXB case. Predicted and measured smoke variation at the chimney.

short-term build up in the concentration of CO_2 and decline in the concentration of O_2 in the room during the fire, Figures 26 and 27. These changes are strongly peaked as the fire is strongly peaked. The return to ambient values however is much slower than in the previous cases, probably due to smouldering by the remains of the boxes. In the early stages of the fire reasonable agreement is obtained between the predicted and measured values for the CO_2 and O_2 concentrations. In the later stages however the agreement is poorer due to the sources going to zero while in reality the fire probably continued to smoulder. Hence the return of the predicted values toward ambient conditions while the measured values do not. This level of agreement in the first stages of the fire is expected as the sources used in the model for these species have been tuned using the experimental measurements. At the chimney, however, the agreement obtained is poorer for both species. This may be due to some experimental error or some phenomenon taking place in the compartment that was not modeled.

For the other combustion products the agreement is generally poorer. The experimental readings for the CO do not give a clear indication as to how the source of this species must be varying in order to produce the readings seen simultaneously at the chimney and in the center of the room. As a compromise a constant yield was used to represent the source term. This was chosen to produce results that are of the correct order of magnitude at both the room center and chimney measuring locations. The generation of the soot was also not clearly understood so again a simple constant yield was used. The results obtained suggest that the yield used is of the right order of magnitude.

As in the other cases these discrepancies can be partially attributed to the modeling of the chimney. The model assumes that any air coming through the chimney from outside has mass concentrations of 23 percent oxygen and 77 percent nitrogen and a temperature of 288 K (ambient). In reality the air that is sucked back through the chimney will be a mixture of ambient air and the exhaust air from the compartment. It will therefore be hotter and will contain some combustion products. This will mix with the air in the compartment and affect both the values measured in the compartment and the values measured in the chimney.

4.3 Conclusion

A numerical model has been developed to aid in the development and optimization of water mist based fire suppression and extinguishment systems. The aim is to provide for industry a tool which can be used to help speed up, and reduce the costs involved in, the design of such systems. The full model includes submodels to simulate the fire, radiation field, water mist, fire suppression, temperature sensors, and the misting nozzle activation system.

This paper presented a description of the overall model structure and a detailed description of the fire and radiation submodels. The fire was represented as a prescribed volumetric source of heat, smoke, CO_2, O_2, and CO and the radiation model was a six flux model. This simplistic approach was selected in order to keep run times to a minimum and because the fuels found in cargo holds are far too complex to be handled by the combustion modeling approaches currently available. The release rates of the combustion products for the fuels of interest required by the model are determined from a series of full-scale experiments.

The comparisons showed good qualitative agreement, the models accurately capturing the trends in the experimental results. Comparisons of predicted and measured temperatures also showed good quantitative agreement. In particular, the measured and predicted temperatures near the compartment ceilings showed excellent agreement. This is an important result as the model is targeted on the development of systems which involve ceiling based fire detection systems. Poorer qualitative agreement was noted for the prediction of CO and smoke. This is partly due to the introduction of considerable uncertainty in the release rates for these products.

The smoke concentration within the compartment has an influence on the predicted temperature field. The sources for the smoke were not well known however and the predictions of the smoke distribution showed poor agreement with the experimental results. It is likely therefore that this uncertainty in the smoke release rates was responsible for a large part of the variation seen between the predicted and measured temperatures, particularly in the lower part of the compartment.

The successful outcome of the fire model development enabled the development of the other key components of the FIREDASS system, namely the mist, extinguishment, and detection/activation models. These are the subject of a later paper.

ACKNOWLEDGMENTS

The FIREDASS programme was sponsored by the European Commission under BRITE-EuRam Framework IV (contract no. BRPR-CT95-0040). The authors would also like to acknowledge the invaluable efforts of their collaborators: BAe Systems; DLR; National Technical University of Athens; Siemens Cerberus; SINTEF NBL; the U.K. Civil Aviation Authority. Finally, Prof. Galea is indebted to the UK CAA for their financial support of his personal chair in Mathematical Modelling at the University of Greenwich.

REFERENCES

1. D. L. Mauzerall, Protecting the Ozone Layer. Phasing Out Halon by 2000, *Fire Journal (Boston), 84,* pp. 22-31, September-October 1990.
2. J. N. Smithies, P. E. Burry, and M. J. Spearpoint, Background Signals from Fire Detectors: Measurement, Analysis, Application, *Fire Safety Journal, 17*:6, pp. 445-459, 1991.
3. FIREDASS—Fire Detection and Suppression Simulation. Task 1.3.2. SINTEF Trials, *FIREDASS report;* Proj. ref. no. 1.3.2, July 1997.
4. The Fire Model Validation Report, *FIREDASS report;* Proj. ref. no. 2.2-4, March 1998.
5. Mist Model—Development, Implementation and Validation, *FIREDASS report;* Proj. ref. no. 3.1.1-2, June 1998.
6. Attenuation of Fire Radiation Through Water Droplets, *FIREDASS report;* Proj. ref. no. 3.1.3-2, April 1997.
7. The Discrete Transfer and the Six Flux Radiation Models on Steckler's Room, *FIREDASS report;* Proj. ref. no. 3.1.3-4, July 1997.
8. Radiation Model Implementation, *FIREDASS report;* Proj. ref. no. 3.1.3-5, February 1997.
9. The Interaction Model Development and Validation Report, *FIREDASS report;* Proj. ref. no. 3.2-1/3.2-2, June 1998.
10. Detection/Activation Model Development and Verification, *FIREDASS report;* Proj. ref. no. 4.2.2-4.3.1-1, July 1998.
11. FIREDASS—Abstract and Results, *FIREDASS report;* DLR doc. no. FD-DS-450-01/0, December 1998.
12. Final Technical Report, *FIREDASS report;* Proj. ref. no. 5.4-1, April 1999.
13. Exploitation Report, *FIREDASS report;* Proj. ref. no. 5.4-2, March 1999.
14. Synthesis Report, *FIREDASS report;* Proj. ref. no. 5.4-4, March 1999.
15. E. R. Galea, FIREDASS—Full Scale Fire Testing, *Presented: FAA International Fire & Cabin Safety Research Conference, Atlantic City, New Jersey, USA;* Nov. 1998; http://fseg.gre.ac.uk/firedass/htmlfile/pubspres.htm.

16. A. J. Grandison, R. N. Mawhinney, E. R. Galea, M. K. Patel, E. P. Keramida, A. G. Boudouvis, and N. C. Markatos, The FIREDASS (FIRE Detection And Suppression Simulation) Model, *FAA International Fire & Cabin Safety Research Conference, Atlantic City, New Jersey, USA,* November 1998, http://www.fire.tc.faa.gov/conference/fire.html, http://fseg.gre.ac.uk/firedass/htmlfile/pubspres.htm.
17. C. Goodchild, FIREDASS—A Fire Detection and Suppression Simulation Research Project, *Air and Space Europe (ISSN 1290-0958), 2*:1, pp. 96-100, 2000.
18. FIREDASS Web site: http://fseg.gre.ac.uk/firedass.
19. S. V. Patankar, *Numerical Heat Transfer and Fluid Flow,* McGraw Hill, New York, 1980.
20. E. R. Galea, On the Field Modelling Approach to the Simulation of Enclosure Fires, *Journal of Fire Protection Engineering, 1*:1, pp. 11-22, 1989.
21. G. Cox (ed.), Combustion Fundamentals of Fire, Academic Press, 1995.
22. A. F. Sarofim, Radiative Heat Transfer in Combustion: Friend or Foe, *Proceedings of the 21st International Symposium on Combustion,* pp. 1-23, 1986.
23. N. Hoffmann and N. C. Markatos, Thermal Radiation Effects on Fire Enclosures, *Applied Mathematical Modelling, 12,* pp. 129-140, 1988.
24. M. F. Modest, Radiative Heat Transfer, McGraw Hill, New York, 1993.
25. B. Spalding, Radiation Heat Transfer in Participating Media, *CHAM, Encyclopaedia PHOENICS 2.1,* 1994.
26. *CFX 4.1 User Guide,* AEA Technology, 1995.
27. R. Wighus, An Empirical Model for Extinguishment of Enclosed Fires with Water Mist, *Presented: HOTWC '98, Albuquerque, New Mexico, USA,* May 1998.
28. Characterisation of the Spray from the GMAv Nozzle, *AEA report;* File ref. no. AEAT-1195, January 1997.
29. C. T. Crowe, M. P. Sharma, and D. E. Stock, The Particle-Source-In Cell (PSI-Cell) Model for Gas-Droplet Flows, *Trans. of ASME Journal of Fluids Engineering,* pp. 325-332, June 1977.
30. R. N. Mawhinney et al., The Development of a CFD Based Simulator for Water Mist Fire Suppression Systems: The Development of the Mist Submodel, in preparation.
31. E. P. Keramida, N. N. Souris, A. G. Boudouvis, and N. C. Markatos, Numerical Modeling of Radiative Heat Transfer in Integrated CFD Fire Modeling, *Journal of Applied Fire Science, 9*:1, pp. 3-19, 2000.
32. E. R. Galea and N. C. Markatos, The Mathematical Modelling and Computer Simulation of Fire Development in Aircraft, *International Journal of Heat and Mass Transfer, 34,* pp. 181-197, 1991.
33. N. C. Markatos and G. Cox, Hydrodynamics and Heat Transfer in Enclosures, *Physico-Chem. Hydrody, 5,* pp. 53-66, 1984.
34. S. Simcox, N. S. Wilkes, and I. P. Jones, Computer Simulation of the Flows of Hot Gases from the Fire at Kings Cross Underground Station, *Fire Safety Journal, 18,* pp. 49-73, 1992.
35. E. R. Galea, D. Berhane, and N. A. Hoffmann, CFD Analysis of Fire Plumes Emerging from Windows with External Protrusions in High-Rise Buildings, *Proceedings of Interflam '96,* pp. 835-839, 1996.
36. L. Kerrison, N. Mawhinney, E. R. Galea, N. Hoffmann, and M. K. Patel, A Comparison of Two Fire Field Models with Experimental Room Fire Data, *Proceedings of the 4th International Symposium on Fire Safety Science,* pp. 161-172, 1994.

37. L. Kerrison, E. R. Galea, N. Hoffmann, and M. K. Patel, A Comparison of a FLOW3D Based Fire Field Model with Experimental Room Fire Data, *Fire Safety Journal, 23,* pp. 387-411, 1994.
38. Z. Wang, F. Jia, E. R. Galea, M. K. Patel, and J. Ewer, Simulating One of the CIB W14 Round Robin Test Cases Using the SMARTFIRE Fire Field Models, CMS Press, Paper no. 00/IM/53 (ISBN 1 899991 54 9), 2000.
39. G. H. Yeoh, V. Chandrasekaran, and E. Leonardi, Numerical Prediction of Fire and Smoke, *AIRAH Journal, 49,* pp. 13-18, 1995.
40. S. Kumar, A. K. Gupta, and G. Cox, Effects of Thermal Radiation on the Fluid Dynamics of Compartment Fires, *Proceedings of the 3rd International Symposium on Fire Safety Science,* pp. 345-354, 1991.
41. Z. Yan and G. Holmstedt, CFD and Experimental Studies of Room Fire Growth on Wall Lining Materials, *Fire Safety Journal, 27,* pp. 201-238, 1996.
42. F. Jia, E. R. Galea, and M. K. Patel, The Prediction of Fire Propagation in Enclosure Fires, *Proceedings of the 5th Symposium on Fire Safety Science,* pp. 35-354, 1997.
43. F. Jia, E. R. Galea, and M. K. Patel, Simulating 'FLASHOVER' and 'BACKDRAFT' Type Events Using Fire Field Models—A First Approximation, *Journal of Fire Protection Engineering, 9,* pp. 1-17, 1997.
44. F. Jia, E. R. Galea, and M. K. Patel, The Numerical Simulation of the Noncharring Pyrolysis Process and Fire Development within a Compartment, *Applied Mathematical Modelling, 23,* pp. 587-607, 1999.
45. G. Heskestad, Peak Gas Velocities and Flame Heights of Buoyancy-Controlled Turbulent Diffusion Flames, *Proceedings of the 18th International Symposium on Combustion,* pp. 951-960, 1981.
46. F. C. Lockwood and N. G. Shah, A New Radiation Solution Method for Incorporation in General Combustion Prediction Procedures, *Proceedings of the 18th International Symposium on Combustion,* pp. 1405-1414, 1981.
47. K. D. Steckler, J. G. Quintiere, and W. J. Rinkinen, Flow Induced by Fire in a Compartment, *U.S. Dept. of Commerce,* NBSIR 82-2520, 1982.
48. The SFPE Handbook of Fire Protection Engineering (2nd Ed.), *NFPA,* pp. 3-78, 1995.

Direct reprint requests to:

R. N. Mawhinney
University of Greenwich
London, SE 10 9LS
United Kingdom